On the dynamics of buoyant jets in a linearly stratified ambient ⊘

Harish N. Mirajkar ✉ ⓘ ; Partho Mukherjee ⓘ ; Sridhar Balasubramanian ⓘ

Check for updates

View Online

Export Citation

Articles You May Be Interested In

Experimental study of horizontal heated buoyant jets in a linearly stratified ambience

Physics of Fluids (April 2021)

Dynamics of a buoyant gravity current propagating in a linearly stratified medium

Physics of Fluids (July 2022)

Hydrodynamics of horizontal heated buoyant jet in linearly stratified fluids

Physics of Fluids (February 2022)

04 December 2024 13:06:08

On the dynamics of buoyant jets in a linearly stratified ambient

View Online   Export Citation   CrossMark

Harish N. Mirajkar,[a] (iD) Partho Mukherjee,[b] (iD) and Sridhar Balasubramanian[c] (iD)

AFFILIATIONS

Geophysical and Multiphase Flow Lab, Indian Institute of Technology Bombay, Mumbai 400076, Maharashtra, India

[a]Present address: Engineering Mechanics Unit, Jawaharlal Nehru Center for Advanced Scientific Research, Bangalore 560064, Karnataka, India. **Author to whom correspondence should be addressed:** harishnmirajkar@gmail.com
[b]Present address: Adani University, Ahmedabad 382421, Gujarat, India.
[c]Also at: Interdisciplinary Program in Climate Studies, Indian Institute of Technology, Bombay, Mumbai 400076, Maharashtra, India.

ABSTRACT

We report mean flow and turbulence characteristics of a buoyant jet evolving in a linearly stratified ambient with stratification strength $N = 0.4 \, \text{s}^{-1}$. The velocity and density fields are captured experimentally using simultaneous particle image velocimetry and planar laser-induced fluorescence technique. We report our findings by strategically choosing four axial locations such that it covers different flow regimes; namely, momentum-dominated region, buoyancy-dominated region, neutral buoyant layer, and plume cap region. The results at these axial locations are presented as a function of the radial co-ordinate to provide a whole field picture of the flow dynamics. From the mean axial velocity and density fields, it is seen that the velocity and the scalar (density) widths are of the same magnitude in the momentum-dominated region but show significant difference in the buoyancy-dominated region and beyond. It is also seen that the axial velocity for the buoyant jet is consistently higher than pure jet at different axial locations due to buoyancy-aided momentum. With the help of turbulent kinetic energy (TKE) budget analysis, it is seen that the shear production (P) and TKE dissipation (ϵ) for a buoyant jet are higher compared to the case of pure jet at different axial locations, cementing the role of buoyancy and stratification on the flow dynamics. Further, it is observed that the buoyancy flux (B) aids and destroys TKE intermittently in the radial direction, and it is at least $O(10^2)$ smaller than P, ϵ, and the mean flow buoyancy flux (F). Finally, the relative strength of the turbulent transport of momentum to that of scalar in the radial direction is quantified using the turbulent Prandtl number, Pr_t. It is seen that $Pr_t \approx 1$ upto the neutral buoyant layer and ≈ 0.6 in the plume cap region. The current set of results obtained from experiments are first of its kind and elucidates various aspects of the flow which hitherto remained unknown and will also prove to be useful in testing numerical simulations for buoyancy-driven flows.

I. INTRODUCTION

A turbulent buoyant jet is defined as a stream of fluid emanating from a source driven by momentum and the density difference between the ambient and the jet fluid.[1] If the ambient in which it is released has a higher density, the buoyant jet evolves indefinitely in space. However, when the ambient is stably stratified, the flow dynamics is significantly different. The buoyant jet fluid rises and simultaneously entrains the ambient fluid leading to its dilution. This process continues up until the point where the jet fluid's and the ambient fluid's densities become equal, and this region is known as the neutral buoyant layer. Though the neutral buoyancy level puts a brake on the flow, the jet by virtue of its inertia shoots past this layer. The jet then abruptly comes to a halt after reaching a maximum height and begins

to spread out horizontally, causing the flow to become two-dimensional.[2] Such flows are often encountered as a result of both anthropogenic activities and natural phenomena. Typical examples include sewage water discharge into water bodies, exhaust gas issuing from industrial chimneys and released into the atmosphere, volcanic eruptions, hydrothermal vents, and so on. Studying the energetics and the dynamical aspects of such flows proves to be a key element in understanding and mitigating air and water pollution. It also equips us with important tools that can often be used to forewarn unfavorable situations and predict its enormity.

The study of turbulent buoyant jets in uniform and stratified environments was pioneered by Morton *et al.*[3] They were the first to derive an empirical relation to find the maximum height, spreading

height of the buoyant jet as a function of source parameters such as volume flux (Q_o), momentum flux (M_o), and buoyancy flux (B_o). Following this study, other researchers tried to quantify the effect of ambient stratification on the radial spreading of buoyant jets (see for e.g., Refs. 4–11). In recent times, Zhang et al.,[12] Mirajkar et al.,[13] and Clément et al.[14] used Particle Image Velocimetry (PIV) to capture the velocity field of a buoyant jet evolving in a stratified ambient and characterized the turbulence using Reynolds stress, turbulent kinetic energy (TKE), and energy spectra. Mukherjee et al.[15] quantified the entrainment dynamics of buoyant jets in a linearly stratified ambient using simultaneous PIV and Planar Laser-Induced Fluorescence (PLIF). Because of the difficulties associated with creating precise and repeatable stratification and the difficulty to deploy instruments in variable density flows (such as refractive index matching), buoyant jets in the stratified environment have not been extensively characterized experimentally.

Major numerical studies pertaining to jets/plumes/buoyant jets started around the turn of the 21st century. Yuan et al.[16] proved to be one such significant piece of work who studied the flow and mixing dynamics of a round jet released in an environment with a cross flow using Large Eddy Simulation (LES). Numerical studies on jets paved way for buoyant jets evolving in a uniform ambient, e.g., Basu and Mansour[17] and Zhou et al.,[18] who studied the entrainment, mean flow, and turbulent characteristics of the turbulent buoyant jet in a uniform medium. Devenish et al.[19] performed LES to study pure plume in uniform and stably stratified ambients. The most significant aspect of their work was that they were able to discover plume top entrainment and detrainment and figured out the mechanisms that significantly affect the mean flow characteristics. Recently, Kumar et al.[20] studied the buoyant jet's behavior in a linearly stratified ambient using the Reynolds Averaged Navier Stokes (RANS) model (which can sometimes be inaccurate for buoyancy-driven flows). They quantified the important terms appearing in the TKE budget equation and reported its variation with the axial distance. Due to the limitation of the current computational power, resolving the whole range of spatial and temporal scales for such buoyancy-driven flows is quite challenging and expensive. For this reason, literature dealing with the numerical investigation of buoyant jets evolving in a stratified ambient that employs LES and Direct Numerical Simulation (DNS) are almost non-existent.

To the best of our knowledge, the detailed experimental study of buoyant jets evolving in a linearly stratified ambient employing simultaneous measurements of velocity–density fields has not been pursued in the past. The earlier experimental studies only used velocity measurements to characterize the flow dynamics. As far as the numerical simulations are concerned, although Kumar et al.[20] reported the TKE budget terms, the quantities were volume averaged and its variation was shown as a function of growing axial distance. These findings should also be supplemented with the variation of the relevant quantities along the radial direction at different axial locations. The evolution in the radial direction is important because it provides a complete picture and aids us in delving deeper into the flow dynamics and its energetics, and this is the central theme of this paper. In this experimental study, we use simultaneous PIV–PLIF to capture the velocity and density fields of a positively buoyant jet (jet's density is less than that of ambient) evolving in a linear stably stratified environment. The mean flow characteristics, such as the axial velocity and density profiles, and

its distribution along the radial co-ordinate (r) at different axial locations are first reported. Subsequently, the important terms appearing in the TKE budget equation are quantified, viz., shear production (P), buoyancy flux (B), and the viscous dissipation (ϵ) (the source and sink terms) as a function of radial distance at different downstream locations. Finally, the turbulent Prandtl number (Pr_t) that shows the relative strength of turbulent transport of momentum to a scalar is quantified. The paper is organized as follows: in Sec. II, experimental setup and techniques are explained. In Sec. III, results from the experiments are discussed. Finally, in Sec. IV, the paper is concluded with key takeaway points from our study.

II. EXPERIMENTAL SETUP AND FLOW DETAILS

The experimental setup mainly consists of a cubical tank (T1) and a cuboidal tank (T2). Tanks T1 and T2 are made of plexiglass, measuring $60 \times 60 \times 60 \, cm^3$ (L × W × H) and $91 \times 91 \times 60 \, cm^3$ (L × W × H), respectively as shown in Fig. 1. Tank T1 acts as a reservoir for storing the jet fluid and tank T2 is where the ambient stratification is created and experiments are carried out. A centrifugal pump is used to discharge the jet fluid into the ambient using a round nozzle having a diameter $D = 1.27 \, cm$ fixed at the bottom of T2. The nozzle is designed in such a way so as to generate a uniform flow velocity at the exit.[21] The mean axial velocity at the nozzle exit is $W_o \approx 0.22 \, ms^{-1}$. For the case of a buoyant jet in a stratified ambient, the reduced gravity is represented as $\tilde{g} = g \frac{\Delta \rho}{\rho_a}$, where g is the acceleration due to gravity and $\Delta \rho = \rho_a - \rho_{bj}$ is the density difference between the local ambient fluid and the buoyant jet fluid. The two most important non-dimensional parameters used in the study are Reynolds number Re and bulk Richardson number (Ri_b). The ratio of inertial to viscous forces is represented by Re, and it stays constant for a free shear flow. The ratio of buoyancy to inertial forces is given as Ri, and it increases with growing axial distance as the buoyancy force starts to dominate the flow (also seen in Talluru et al.[22]). The values of these non-dimensional parameters and its mathematical formulation together with the experimental parameters are shown in Table I.

A. Ambient stratification

A linear stable density stratification in the experiments is created using a double bucket system[23] that uses a combination of commercial salt, isopropanol, and water such that the heavier fluid ($\rho_b = 1002.4 \, kg \, m^{-3}$) is at the bottom of the tank and lighter fluid ($\rho_t = 996.7 \, kg \, m^{-3}$) stays at the top. The reason isopropyl alcohol is added to B1 is to avoid aberrations in the image when we use optical diagnostic techniques such as PIV–PLIF.[24,25] The details of the density variation of the solution as a function of solute concentration and respective refractive index matching are shown graphically in Fig. 2. A double bucket system mainly consists of two buckets (B1 and B2) as shown in Fig. 1. Bucket B1 is filled with a mixture of water and isopropanol solution, while B2 is filled with the heavier salt water solution. In order to create a linear stratification, fluid is flown from B1 into B2 at a flow rate Q and from B2 into the experimental tank (T2) at a flow rate $2Q$. The solution in B2 is continuously mixed using a motor-controlled stirrer. Tank T2 is filled by pouring the fluid over a perforated wooden plate. Once the fluid is filled up to a height of $H = 40 \, cm$, the perforated wooden plate is removed carefully such that it creates a minimal disturbance that can disrupt the stratification. Before each experimental run, fluid samples are collected from tank
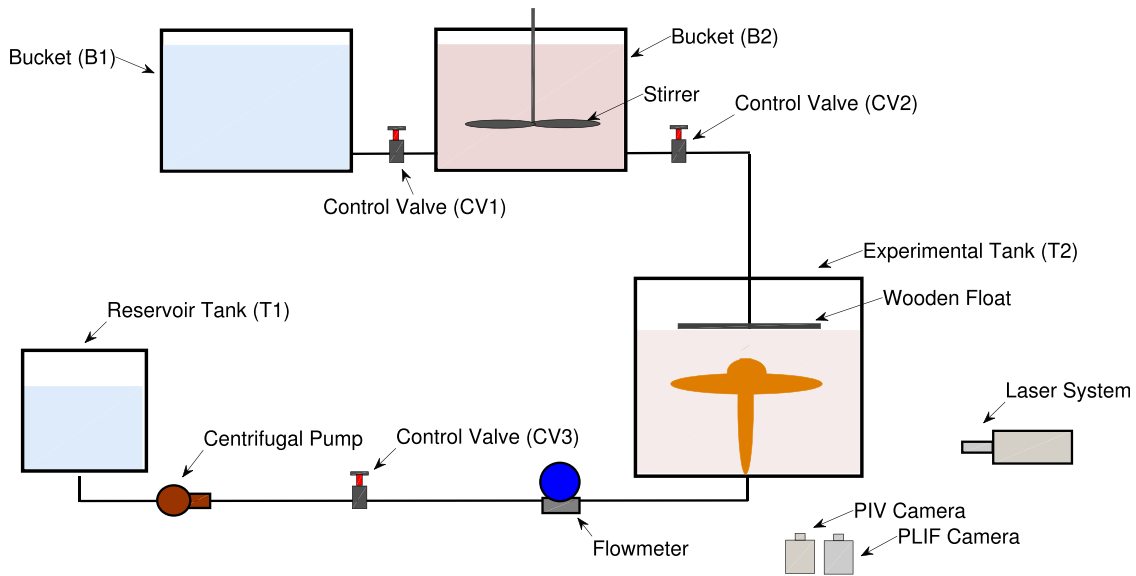
FIG. 1. Schematic of the experimental setup.

T2 at every 1 cm interval from the bottom till the free surface (i.e., 40 cm). The densities of the samples are measured using a portable densitometer (manufacturer: Antonpaar). The resultant ambient stratification created using this method is shown in Fig. 3.

B. PIV system

Particle Image Velocimetry (PIV) is used for capturing the velocity field over a period of time as illustrated in Fig. 1 (illuminated region of interest). An Nd:YAG double pulse laser (532 nm, maximum intensity 145 mJ pulse) is used for visualizing the flow field. The laser beam is expanded into a 1 mm thin laser sheet illuminating the region of interest in the $r - z$ plane such that the jet centerline lies in the illuminated plane. The jet fluid and the ambient fluid are uniformly seeded with polyamide tracer particles (median diameter 55 μm, specific gravity 1.1) to track the flow field. In order to achieve high spatial resolution, the entire axial span was divided into four different regions of interest (RoI) as shown in Fig. 4. The time delay (Δt) between the two pulses in the PIV camera is set for 2.3, 4, 7, and 9 ms for the four different RoI. The maximum displacement of the particle is six pixels between two frames in order to maintain a dynamic range, DR >10, in each layer. A CCD camera with a resolution of 1392 × 1080 pixels focused on each RoI measuring approximately 10 × 9 cm² with a spatial resolution of 0.05 cm/pixel. The PIV spatial resolution (Δ) in this study is close to 1 mm, and it is almost two to three times the Kolmogorov length scale (L_κ) which helps in the accurate estimation of viscous dissipation. An image acquisition and laser control system is used to synchronize the measurements with a sampling rate of 5 Hz.

TABLE I. Initial parameters in the experiments.

| Parameter		Pure jet	Buoyant jet
Jet mean velocity (ms^{-1})	W_o	0.22	0.22
Bottom density in T2 (kg m^{-3})	ρ_b	997.8	1002.4
Top density in T2 (kg m^{-3})	ρ_t	997.8	996
Reynolds number	$\dfrac{\rho W_o D}{\mu}$	3100	3100
Source Richardson number	$\left(\dfrac{\pi}{4}\right)^{0.25}\sqrt{\dfrac{\tilde{g}D}{W_o^2}}$	$\cdots$	0.1
Volume flux (m^{4}s^{-1})	$\dfrac{1}{4}\pi D^2 W_o$	2.8×10^{-5}	2.8×10^{-5}
Momentum flux (m^{4}s^{-2})	$Q_o W_o$	6.1×10^{-6}	6.1×10^{-6}
Buoyancy flux (m^{4}s^{-3})	$g' Q_o$	$\cdots$	1.5×10^{-6}
Buoyancy frequency (s^{-1})	$N=\sqrt{-\dfrac{g}{\rho_b}\dfrac{\partial \rho}{\partial z}}$	$\cdots$	0.4
Morton length scale (m)	$M_o^{3/4}B_o^{-1/2}$	$\cdots$	0.1
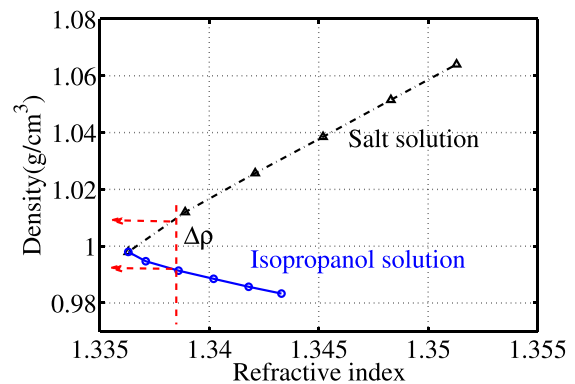
FIG. 2. Densities and refractive indices of isopropanol and salt solutions. The measured data show a linear fit.
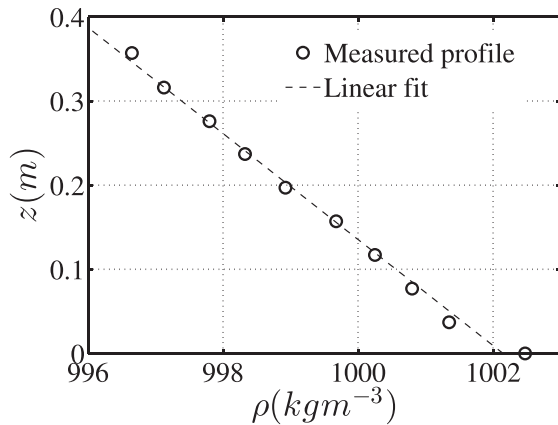
FIG. 3. Ambient density profile in the experiment tank (T2).

The PIV images are captured at a frame rate of 5 fps, and the measurement time was 180 s which is sufficient for time averaging the quantities since the flow is in a steady state. The data are processed on PIVlab using MATLAB application software. Based on the cross correlation algorithm, we employ a two-step iteration algorithm with an interrogation window of 64×64 pixels and a sub-window of 32×32 pixels.

C. PLIF system

Planar Laser-Induced Fluorescence (PLIF) is employed to obtain a density field over a period of time in the present experiments. Rhodamine 6G (R6G) is used as the fluorescent dye in the experiments. The R6G had peaks of absorption and emission spectrum of around 550 nm, respectively. The dyed fluid is illuminated by Nd:YAG laser having a wavelength 532 nm, and the images are recorded by a CCD camera, with a resolution of 1040×1360 pixels. A low-pass filter lens with a cutoff wavelength 550 nm is attached to the camera for filtering out the green reflected light from PIV particles. The PLIF camera is mounted on schuflug mounting in order to adjust and visualize the same region of interest as captured by the PIV camera. Both the
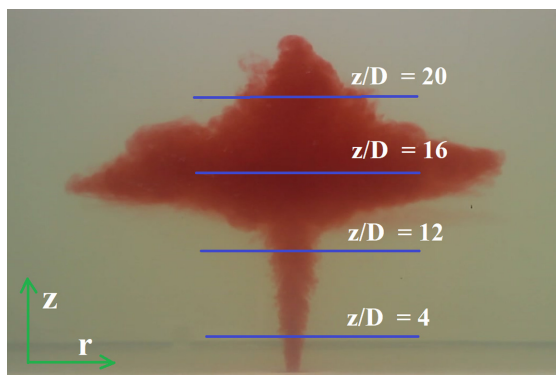

FIG. 4. Representation of a buoyant jet in a linear stably stratified ambient through a simple dye experiment. The locations at which the results are reported in this study are indicated.

PIV and PLIF cameras are triggered at the same time using a synchronizer to achieve simultaneous measurements of velocity and density fields.

The dye is mixed uniformly in each of the double bucket tanks ($\approx 40\,\mu\text{gm/L}$ in each bucket) before creating the density stratification. The jet fluid or the fluid in tank T1 has $0\,\mu\text{gm/L}$ concentration of R6G. Before the start of the experiments, the background gray image is captured to get the initial intensity (I_1) of the ambient fluid. The experiments are commenced by releasing the jet fluid into the ambient fluid, and as the jet fluid mixes with the ambient fluid and dilutes, the density field now has a reduced intensity I_2. Using these intensities, we quantify the instantaneous density field using the relation shown below. Detailed discussion on the calibration technique is explained in Balasubramanian and Zhong.[11]

$$\rho = \rho_{bj} - \frac{I_1}{I_2}(\rho_2 - \rho_1). \qquad (1)$$

Here, I_1 is the initial intensity of the ambient stratified fluid (i.e., background image). Upon the release of the jet fluid into the ambient stratified fluid, entrainment occurs, causing a change in the local intensity which is I_2 and ρ_{bj} is the density of the buoyant jet fluid. The errors associated with the calculation of the density values are estimated to be $\pm 5\%$, which is mainly associated with the calculation of the density using Eq. (1).

III. RESULTS AND DISCUSSION

In this section, we present the mean flow and turbulence characteristics of a buoyant jet evolving in a stably stratified ambient. In order to gain better insights and gauge the effect of buoyancy and stratification on the flow dynamics, the results are compared with that of a pure jet (the ambient and the jet densities are equal). To reiterate, our objective is to provide the whole field measurement at critical axial locations that encompass different flow regimes. We have chosen four such critical axial locations: (a) near source region (momentum dominated) ($z/D = 4$), (b) buoyancy-dominated region ($z/D = 12$), (c) near neutral buoyant layer ($z/D = 16$), and (d) region above the neutral layer or plume cap region ($z/D = 20$). The details of the case study are as follows:

1. Pure jet (PJ): Density of the ambient and the jet fluid is equal ($\rho_j = \rho_a = 997.8\,\text{kg m}^{-3}$).
2. Buoyant jet (BJ): Ambient is stably stratified with buoyancy frequency, $N = 0.4\,\text{s}^{-1}$, and the jet fluid has a density of $\rho_{bj} = 995.7\,\text{kg m}^{-3}$.

In this study, an instantaneous field variable is represented as X, its time-averaged value is represented as $\langle X \rangle$, and its fluctuating component is represented as $X - \langle X \rangle = X'$.

A. Mean velocity field

Figures 5(a) and 5(b) illustrate mean axial velocity of the pure jet and buoyant jet, respectively, as a function of radial co-ordinate at different axial locations from the source. As the jet evolves, it is seen from Fig. 5(a) that the mean velocity decreases with increasing axial distance. Pure jet is energy conserving, yet there is a reduction in the mean velocity with growing axial distance because the jet spreads or widens as a result of entrainment of the ambient fluid. There is a
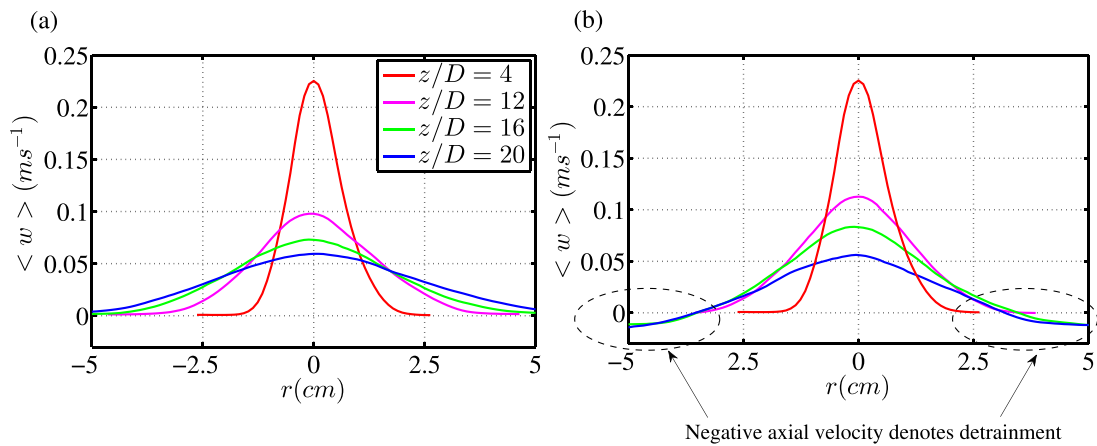
FIG. 5. Axial velocity profiles as a function radial distance at different axial locations for the (a) pure jet and (b) buoyant jet.

constant momentum transfer between the jet and the ambient, and an increase in width is compensated with a decrease in axial velocity. Figure 5(b) illustrates the mean velocity field as a function of radial co-ordinate for a buoyant jet evolving in a stably stratified ambient. Qualitatively, the mean axial velocity and its behavior with growing axial distance are similar to that of the pure jet, but as the buoyant jet moves to a buoyancy-dominated region, the features become strikingly different. The mean momentum and energy of the flow in this case are supplemented by a positive buoyancy force till the neutral layer. As a result of this, the velocity at axial locations $z/D = 12, 16$ is higher in the case of the buoyant jet as compared to the pure jet. Another feature that can be noticed is the presence of detrainment when the buoyant jet approaches the neutral layer. A negative axial velocity is a representation of the detrainment process. However, it is localized to the edge of the buoyant jet as evident from the velocity profiles at $z/D = 16, 20$. The axial velocity is not negative for the entire buoyant jet width but closer to its edge. Beyond the neutral layer, the mean

axial velocity of the buoyant jet drops to zero at an axial location $z/D = 24$ (the maximum height reached), whereas the pure jet's mean velocity keeps decreasing and asymptotically approaches zero. In Fig. 6, we show axial velocity contour plots to complement the earlier discussion. Qualitatively, we can notice a bulbous or a plume cap region above the neutral layer for the buoyant jet case indicating that the velocity has abruptly reached zero. Whereas, in the case of pure jet, there is no cap region and it keeps growing indefinitely.

B. Mean density plot

Figure 7 illustrates non-dimensionalized mean density plots for the buoyant jet as a function of radial co-ordinates at different axial locations from the source. For each axial distance, the density is non-dimensionalized using the local ambient density. This non-dimensional form effectively captures the degree of dilution as the buoyant jet evolves in space. The entire buoyant jet, including its
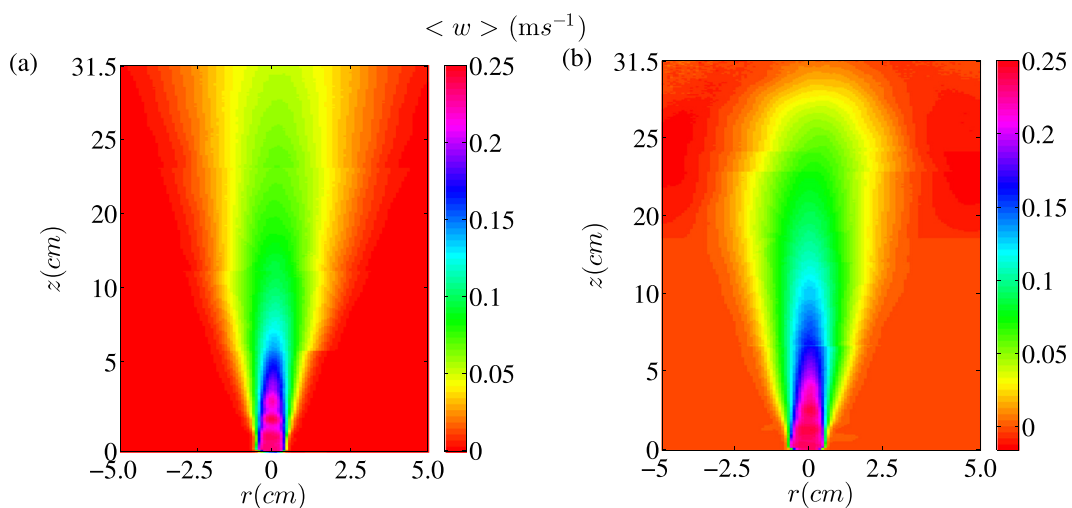

FIG. 6. Mean axial velocity contour plots for the (a) pure jet and (b) buoyant jet.
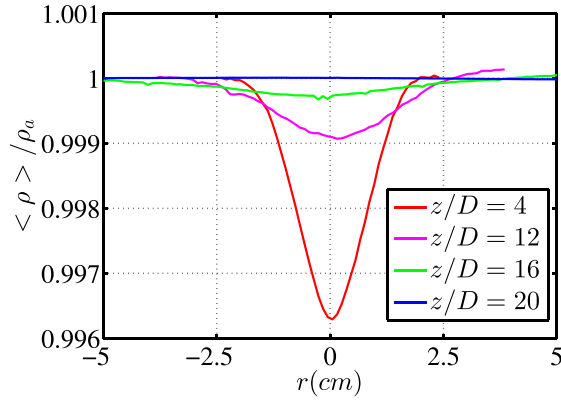
FIG. 7. Normalized mean density profile as a function radial distance at different axial locations for the buoyant jet.

center, begins to get diluted the moment it is released in the ambient fluid. The numerical values across the radial direction are an indication of how the jet density approaches the local ambient density. It is seen from the figure that the dilution is non-uniform, and it is higher at the jet edges compared to the core, especially in the momentum-dominated region. However, the dilution process progressively becomes more uniform in the buoyancy-dominated region and beyond. This argument is reinforced if we compare the radial distribution of density at $z/D = 4$ and $z/D = 12, 16$. At $z/D = 12, 16$, the entire jet's density collectively approaches the local ambient density, compared to the location at $z/D = 4$, where the degree of dilution is lot higher at the edges compared to the center. At $z/D = 20$, above the neutral layer, complete dilution of the jet fluid has happened, and the entire jet's density is almost equal to the local ambient density. Another novel observation from the mean density plots is that the scalar width is almost the same as that of the velocity width in the momentum-dominated region. But, as we move to the buoyancy-dominated region and beyond, the scalar width has a slightly higher value and almost approaches infinity near the neutral layer. The velocity width, however, increases but is consistently less than the scalar width in the buoyancy-dominated region. Near the neutral layer, the velocity width actually starts reducing (also observed in Mukherjee et al.[15]).

C. Turbulent characteristics

In our previous paper,[13] using only the velocity field, turbulence statistics such as Reynolds stress, turbulent kinetic energy (TKE), and turbulence intensity is reported. In our current study with the help of simultaneous velocity and density measurement, we can now quantify the turbulent density flux. This helps in understanding the budget equation in much more detail and to quantify the turbulent transport of momentum and scalar.

1. Turbulent kinetic energy (TKE) budget

The turbulent kinetic energy budget equation is given as Kundu et al.[26]

$$\frac{\partial k}{\partial t} + \langle u_i \rangle \frac{\partial k}{\partial x_i} = Tr + P - B - \epsilon, \tag{2}$$

where k is the TKE and $\langle u_i \rangle$ is the mean velocity in the i direction responsible for advecting the flow properties. The left-hand side of the equation represents the total time derivative of TKE and is a measure of unsteadiness of the flow. The temporal change in TKE (first term) is zero in the present case, whereas the second term is the convective change, and it is non-zero in the present case since there are spatial gradients of TKE present. The first term on the right-hand side is the divergence which is again zero for homogeneous turbulence. It is responsible for the transport (Tr) of turbulent kinetic energy through turbulent pressure fluctuations, viscous diffusion, and turbulent stress. The second, third, and fourth terms are the actual source and sink of TKE that actively participate in the energetics of the flow and are various mechanisms through which TKE is created or destroyed. The second term is shear production (P), the rate at which the TKE is derived from the mean flow. The third term is the buoyancy flux (B) and represents the small-scale mixing event, and the fourth term is the viscous dissipation (ϵ) which is the rate at which the TKE is getting converted into heat through viscous effects. The terms appearing on the right-hand side of the equation are mathematically represented as follows:[27]

$$P = -\langle u'^2 \rangle \frac{\partial \langle u \rangle}{\partial r} - \langle u'w' \rangle \frac{\partial \langle w \rangle}{\partial r}$$
$$- \langle u'w' \rangle \frac{\partial \langle u \rangle}{\partial z} - \langle w'^2 \rangle \frac{\partial \langle w \rangle}{\partial z}, \tag{3}$$

$$B = \frac{g}{\rho_b} \langle \rho' w' \rangle, \tag{4}$$

$$\epsilon = \nu \left[4 \left\langle \frac{\partial w'^2}{\partial z} \right\rangle + 4 \left\langle \frac{\partial u'^2}{\partial r} \right\rangle + 4 \left\langle \frac{\partial w'}{\partial z} \frac{\partial u'}{\partial r} \right\rangle \right.$$
$$\left. + 3 \left\langle \frac{\partial u'^2}{\partial z} \right\rangle + 3 \left\langle \frac{\partial w'^2}{\partial r} \right\rangle + 6 \left\langle \frac{\partial u'}{\partial z} \frac{\partial w'}{\partial r} \right\rangle \right], \tag{5}$$

$$Tr = \frac{\partial}{\partial x_j} \left[-\frac{1}{\rho_0} \langle p' u'_j \rangle + 2\nu \langle u'_i s'_{ij} \rangle - \frac{1}{2} \langle u'^2_i u'_j \rangle \right]. \tag{6}$$

Here, $\langle u \rangle$ and $\langle w \rangle$ represent the mean (time averaged) radial and axial velocities, and u' and w' represent the respective fluctuating components. Similarly, $\langle \rho \rangle$ is the mean density field and ρ' is its fluctuating component. In the expression for the Tr term, ρ_b is the bottom density of the tank (see Table I), p' is fluctuation in the pressure field, and $s_{ij'}$ is the fluctuation strain rate tensor. Quantifying the Tr term proves to be a stern challenge, and therefore, the usual practice is to quantify the other terms appearing in the equation and infer Tr indirectly. Odier et al.[28] have shown that when $\frac{\Lambda}{L_\kappa} \leq 4$ (for notations refer to Sec. II B), the viscous dissipation can be experimentally resolved to a good extent within the statistical error limit. The 3D viscous dissipation using a 2D velocity field is estimated using Eq. (5) (see Doron et al.[29]).

In Figs. 8(a), 8(c), 8(e), and 8(g), shear production (P) and viscous dissipation (ϵ) are shown for the pure jet at axial locations $z/D = 4, 12, 16, 20$. Near the source $z/D = 4$, turbulence is highly inhomogenous in its developing stages, as seen in Fig. 8(a). The magnitude of P and ϵ is very different indicating that transport and advective terms in the TKE budget equation have an important role to play when the turbulence is developing. The off-center peaks in the r direction about the center indicates that a particular quantity peaks along a
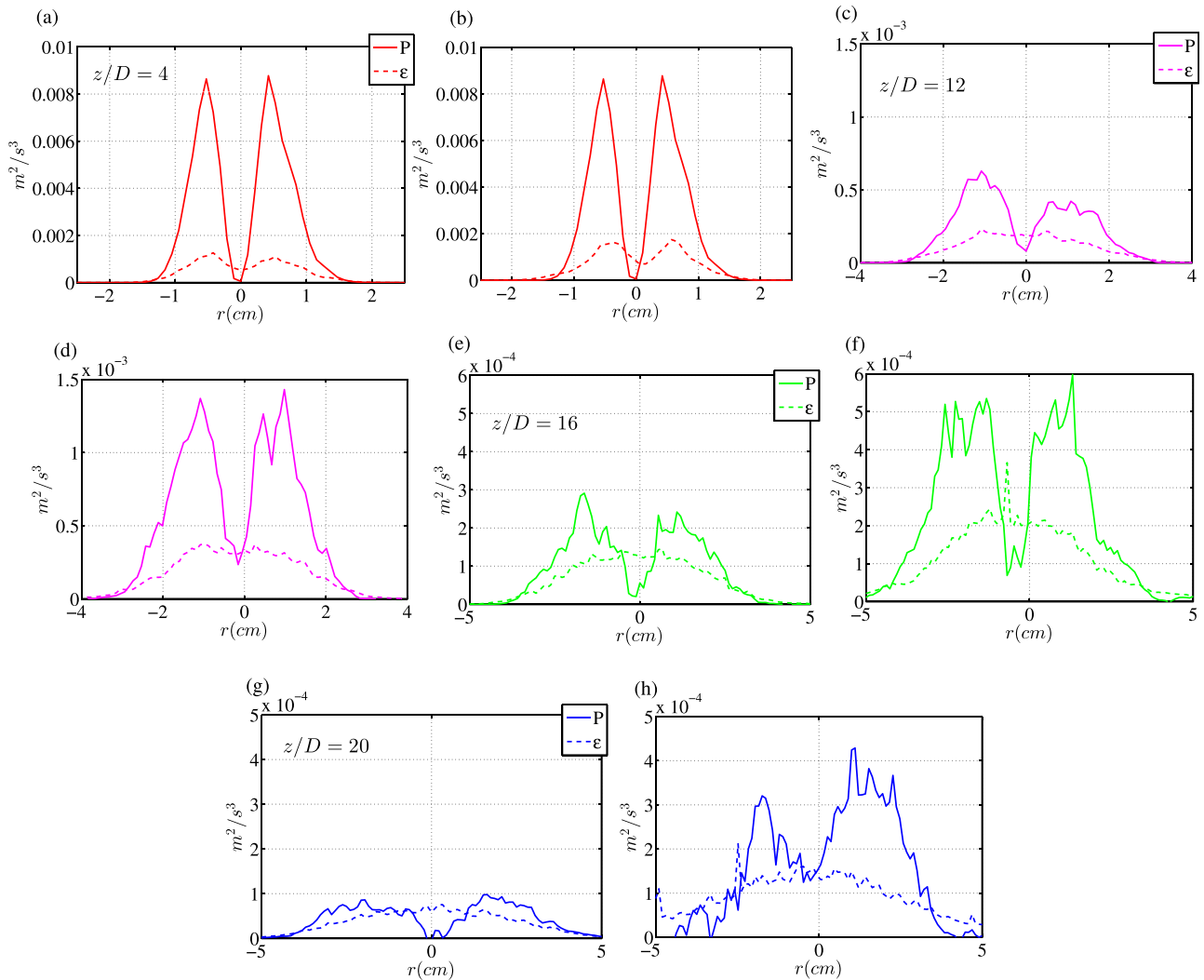
FIG. 8. Shear production (P) and TKE dissipation (ϵ) for a pure jet (a), (c), (e), and (g) and buoyant jet (b), (d), (f), and (h) at the different downstream locations.

rim around the jet center. This feature is observed at a location where the velocity gradient is the highest. As we move away from the source [$z/D = 12, 16$, Figs. 8(c) and 8(e)], though the off-center peak feature is maintained, the magnitudes of P and ϵ keep reducing monotonically. Further, the magnitudes of P and ϵ are almost in a balance at an axial location of $z/D = 20$. The results indicate that the advective and the transport terms have little role to play in this region, and the turbulence is more homogenous in nature. One interesting feature noticed here is that P maintains its off-center peak feature at all the axial locations, but ϵ loses this feature in the regions away from the source. The entire jet width (including the centerline) dissipates its TKE in a uniform manner as evident from Figs. 8(c), 8(e), and 8(g).

In the case of the buoyant jet, the qualitative features of the variation of P and ϵ along the radial direction are very similar to that of the pure jet except for some differences. First, the quantitative values of P and ϵ at different axial locations once the buoyant jet moves to a buoyancy-dominated regime (from $z/D = 12$ onwards) are consistently higher than the pure jet. Only in the momentum-dominated region, especially when the turbulence is developing ($z/D = 4$), the values of P for buoyant jet [Fig. 8(b)] and pure jet are of similar magnitudes. Second, P in the case of buoyant jet has some finite value near the buoyant jet center unlike in the case of pure jet. This indicates that the effect of buoyancy-dominated turbulence penetrates till the core of the jet. Third, the balance between P and ϵ is practically absent for the entire axial span of the buoyant jet [Figs. 8(b), 8(d), 8(f), and 8(h)] because of the inhomogeneity and non-stationarity conditions created by introducing stable stratification. Finally, in the plume cap region [Fig. 8(h)], though the mean velocity has significantly reduced, the fluctuations and the chaotic motion in this region give rise to abnormally high values of P and ϵ.

In the TKE budget equation, the buoyancy flux (B) can either act as a sink or a source of TKE depending on whether the flux is
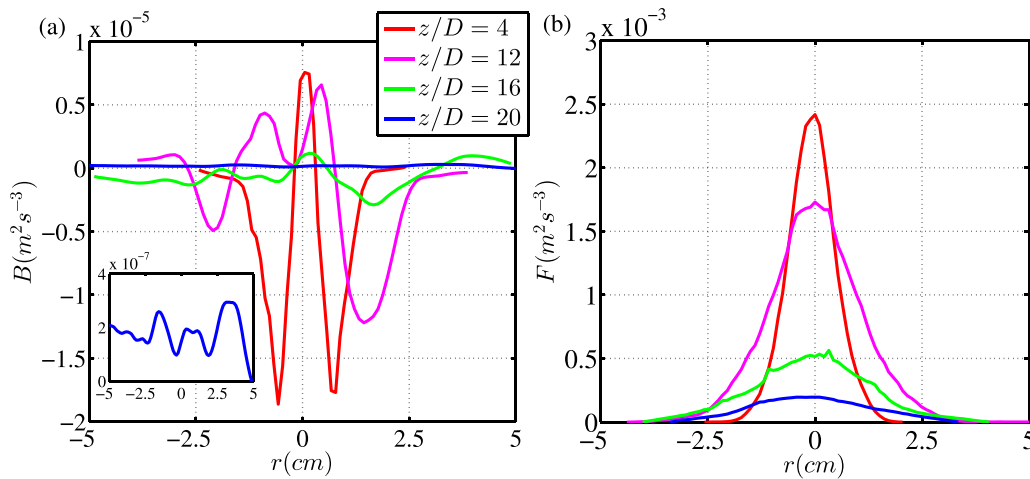
FIG. 9. Turbulent buoyancy flux (B) [shown in (a)] and mean flow buoyancy flux (F) [shown in (b)] profiles at different axial locations. The inset in (a) shows B at an axial location $z/D = 20$ (shown in blue).

irreversible or reversible. Figure 9(a) illustrates B for the case of buoyant jet as a function of radial co-ordinate at different axial locations. This provides a complete picture and identifies zones where B is adding to turbulence or destroying it. These details usually get suppressed when the quantities are presented in a volume-averaged sense (Kumar et al.[20]). First feature that is evident is the absence of well-defined off-center peaks when the buoyant jet has moved to a buoyancy-dominated regime (from $z/D = 12$ onwards) indicating its non-stationary and inhomogenous nature. Second, it is seen that the B adds to TKE and destroys it intermittently across the radial direction, and the randomness in this process increases further in the buoyancy-dominated region. Cumulatively though, B adds to TKE if it is interpreted in a spatially averaged sense along the radial direction (as seen in Kumar et al.[20]). Third and a very important observation is that the magnitude of B at every axial location is considerably lower than P and ϵ (at least 2 orders of magnitude). This signifies that the reason that the TKE is higher in the buoyant jet as compared to the pure jet is because the mean flow buoyancy flux ($F = \tilde{g}\langle w \rangle$) aids the mean flow kinetic energy which then gets converted to TKE via the shear production (P). The mean flow buoyancy flux is plotted as a function of radial co-ordinate at different axial locations in Fig. 9(b), and its order of magnitude is the same as that of P and ϵ. Therefore, it signifies that B is responsible for small-scale mixing and turbulent transport of scalar, but F is responsible for large-scale circulation that energizes the mean flow.

D. Turbulent Prandtl number

Analogous to its molecular counterpart, the turbulent Prandtl number (Pr_t) is the ratio of turbulent diffusion of momentum to that of turbulent diffusion of scalar. In the case of oceanic flows, the vertical eddy diffusivities of momentum and scalar and its parameterizations are quite important. In a similar light, the turbulent transport of momentum and scalar in the radial direction of a buoyant jet is of prime importance. The quantified values of eddy diffusivities of momentum and scalar and an estimate of Pr_t for a buoyant jet

evolving in a stratified ambient are reported for the first time and provide a closure to the discussion on turbulence statistics. The eddy diffusivity of the momentum (κ_m) is the ratio of the Reynolds stress and the mean velocity gradient in the r direction, and the eddy diffusivity of scalar (κ_ρ) is the ratio of the turbulent density flux and the mean density gradient in the r direction. The turbulent Prandtl number is the ratio of these two quantities, and it is represented as

$$Pr_t = \frac{\kappa_m}{\kappa_\rho} = -\frac{\langle u'w' \rangle}{\frac{\partial \langle w \rangle}{\partial r}} \bigg/ -\frac{\langle \rho'u' \rangle}{\frac{\partial \langle \rho \rangle}{\partial r}}. \quad (7)$$

In Fig. 10, the values of κ_m and κ_ρ are shown for different axial locations of the buoyant jet as a function of radial co-ordinate, and an estimate for the value of Pr_t is made. The values of κ_m and κ_ρ are shown on the same plot to gauge the relative strength of one compared to the other. The region close to the source ($z/D = 4$) or the momentum-dominated region, both κ_m and κ_ρ are of the order of $O \approx 10^{-5}$ and similar to the second-order turbulence statistics, the off-center peak feature is maintained. In the buoyancy-dominated region ($z/D = 12$) and the region near the neutral layer ($z/D = 16$), κ_m and κ_ρ are of the order of $O \approx 10^{-4}$, whereas in the plume cap region ($z/D = 20$), κ_m and κ_ρ are of the order of $O \approx 10^{-3}$. The increment in the values of κ_m and κ_ρ with growing axial distance indicates the enhanced turbulent transport of momentum and scalar in the radial direction. Interestingly though, the relative strength of these two given as Pr_t (shown in Fig. 11) almost stays invariant till the neutral buoyant height, and it is approximately equal to 1. Above the neutral layer, in the plume cap region, the Pr_t value drops considerably, and it is approximately equal to 0.6 signifying that the scalar transport is much more dominant in this region compared to the momentum transport. From the above discussion, we can argue that stable stratification and buoyancy effect have a peculiar role in small-scale mixing and enhancing turbulent transport. The estimates of diffusivities and turbulent Prandtl number for buoyant jets in a stratified ambient have not been reported in the past, and they can prove to be useful in numerical
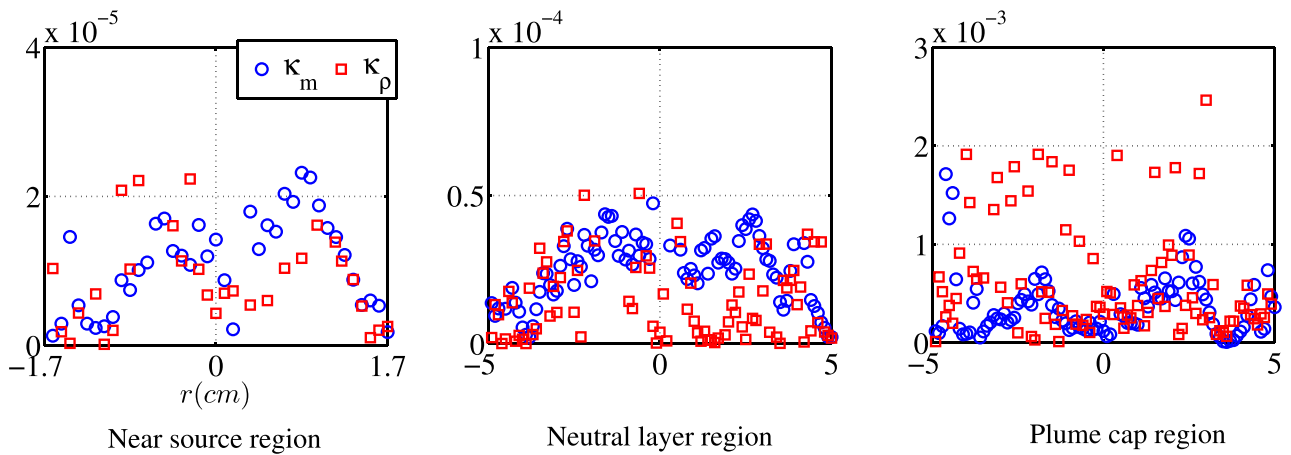
FIG. 10. Variation of eddy diffusivity of momentum and scalar across the radial direction for different buoyant jet regions.
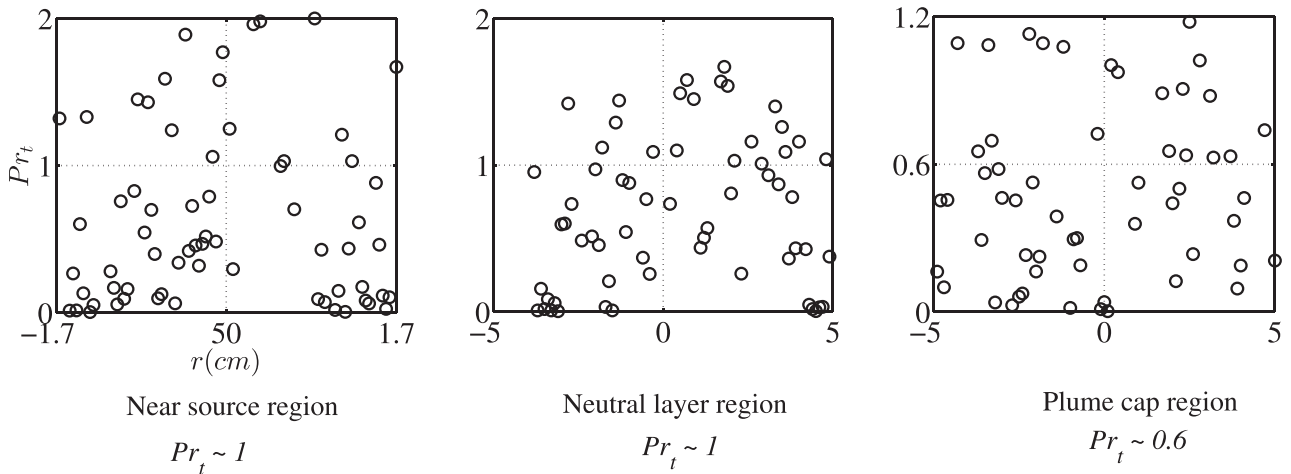

FIG. 11. An estimate of the turbulent Prandtl number (Pr_t) across the radial direction for different buoyant jet regions.

simulations of buoyancy-driven flows. The scatter in the data seen in Figs. 10 and 11 is inevitable because the gradients of fluctuation field variables are obtained from the experiments, but nonetheless, an average estimate of eddy diffusivities and Prandtl number shown here and its variation along the jet width will prove to be useful.

IV. CONCLUSIONS

In this paper, the mean flow and turbulence characteristics of a buoyant jet evolving in a stratified ambient have been investigated using simultaneous measurements of velocity and density field. The results are compared with that of a pure jet to understand the effect of stratification and buoyancy on the jet evolution. We chose four axial locations (momentum-dominated, buoyancy-dominated, near neutral layer, plume cap region) to cover different flow regimes, and the quantities of interest were shown as a function of radial co-ordinate to provide a whole field picture. The important finding from these study has that been results are summarized next.

From the mean velocity plots, we observed that the velocity field's evolution is qualitatively the same for the pure jet and buoyant jet up to the neutral buoyant layer. The regions near the neutral layer and beyond, detrainment occurs, localized at the edge of the buoyant jet, whereas for the same axial location, the mean velocity keeps decaying and asymptotically tries to reach zero. Quantitatively, the magnitude of axial velocity for the case of the buoyant jet was consistently higher compared to that of the pure jet case. From the mean density plots, we could compare the velocity and the scalar widths, and we observed that they were almost of similar magnitudes in the momentum-dominated region but vastly different in the buoyancy-dominated region and beyond.

From the TKE budget analysis, we observed that introducing buoyancy and stratification effects makes the flow highly inhomogenous in nature. Near the source, the shear production (P) and TKE dissipation (ϵ) are of the same magnitude for both the pure jet and buoyant jet. However, in the buoyancy-dominated region and beyond,

P and ϵ have a higher magnitude for the case of the buoyant jet compared to the pure jet. We also observed that the buoyancy flux (B) is at least $O(10^2)$ less than P and ϵ, and it is the buoyancy flux appearing in the mean kinetic energy equation (F) that has the same order of magnitude as that of P and ϵ. This result pointed to the fact that it is F that energizes the turbulence activity and B has a little role to play in enhancing turbulence but is relevant only to the small-scale mixing events.

Finally, the momentum and scalar transport and their relative strength for the case of the buoyant jet are quantified using scalar diffusivities of momentum (κ_m) and scalar (κ_ρ) and the turbulent Prandtl number (Pr_t). Though the values of κ_m and κ_ρ increase with growing axial distance, their relative strength, viz. Pr_t, remains almost unaltered and is close to 1 up until the neutral buoyant height. Beyond this height, in the plume cap region, the Pr_t value drops significantly and is approximately equal to 0.6 indicating a higher rate of scalar transport compared to momentum transport.

The experimental results presented here are first of its kind and reveal vital information regarding the energetics and dynamical aspects of the buoyant jet evolving in a stratified ambient. These results most definitely can be used as a benchmark solution for numerical simulations handling buoyancy-driven flows that can tackle much more complicated problems that are beyond the realm of experiments.

ACKNOWLEDGMENTS

AUTHOR DECLARATIONS
Conflict of Interest

The authors have no conflicts to disclose.

Author Contributions

Harish N. Mirajkar: Conceptualization (equal); Data curation (equal); Investigation (equal); Methodology (equal); Visualization (equal); Writing – original draft (equal); Writing – review & editing (equal). **Partho Mukherjee:** Conceptualization (equal); Formal analysis (equal); Validation (equal); Visualization (equal); Writing – original draft (equal); Writing – review & editing (equal). **Sridhar Balasubramanian:** Funding acquisition (equal); Investigation (equal); Project administration (equal); Resources (equal); Supervision (equal); Validation (equal); Writing – review & editing (equal).

DATA AVAILABILITY

The data that support the findings of this study are available from the corresponding author upon reasonable request.

REFERENCES

[1] B. Morton, "Forced plumes," J. Fluid Mech. **5**, 151–163 (1959).

[2] J. S. Turner, *Buoyancy Effects in Fluids* (Cambridge University Press, 1979).

[3] B. R. Morton, G. I. Taylor, and J. S. Turner, "Turbulent gravitational convection from maintained and instantaneous sources," Proc. R. Soc. London, Ser. A **234**, 1–23 (1956).

[4] L.-N. Fan, "Turbulent buoyant jets into stratified or flowing ambient fluids," Ph.D. thesis (California Institute of Technology, 1967).

[5] N. Kotsovinos, "Axisymmetric submerged intrusion in stratified fluid," J. Hydraul. Eng. **126**, 446–456 (2000).

[6] K. Konstantinidou and P. N. Papanicolaou, "Vertical round and orthogonal buoyant jets in a linear density-stratified fluid," in *Proceedings of XXX IAHR Congress on Water Engineering and Research in a Learning Society: Modern Developments and Traditional Concepts*, edited by J. Ganoulis and P. Prinos (Inland Waters: Research, Engineering and Management Theme, 2003), Vol. 1, pp. 293–300.

[7] N. Kaye, "Turbulent plumes in stratified environments: A review of recent work," Atmos.-Ocean **46**, 433–441 (2008).

[8] P. Papanicolaou and G. Stamoulis, "Spreading of buoyant jets and fountains in a calm, linearly density-stratified fluid," in *Environmental Hydraulics* (2010), pp. 123–128.

[9] T. S. Richards, A. Quentin, and R. B. Sutherland, "Radial intrusions from turbulent plumes in uniform stratification," Phys. Fluids **26**, 036602 (2014).

[10] H. N. Mirajkar, S. Tirodkar, and S. Balasubramanian, "Experimental study on growth and spread of dispersed particle-laden plume in a linearly stratified environment," Environ. Fluid Mech. **15**, 1241–1262 (2015).

[11] S. Balasubramanian and Q. Zhong, "Entrainment and mixing in lock-exchange gravity currents using simultaneous velocity-density measurements," Phys. Fluids **30**, 056601 (2018).

[12] W. Zhang, Z. He, and H. Jiang, "Scaling for turbulent viscosity of buoyant plumes in stratified fluids: PIV measurement with implications for submarine hydrothermal plume turbulence," Deep Sea Res., Part I **129**, 89–98 (2017).

[13] H. N. Mirajkar, P. Mukherjee, and S. Balasubramanian, "PIV study of the dynamics of a forced plume in a stratified ambient," J. Flow Visualization Image Process. **27**, 29–45 (2020).

[14] S. A. Clément, M. A. André, and P. M. Bardet, "Multi-spatio-temporal scales PIV in a turbulent buoyant jet discharging in a linearly stratified environment," Exp. Therm. Fluid Sci. **129**, 110429 (2021).

[15] P. Mukherjee, H. N. Mirajkar, and S. Balasubramanian, "Entrainment dynamics of buoyant jets in a stably stratified environment," Environ. Fluid Mech. **2022**, 1–23 (2022).

[16] L. L. Yuan, S. L. Robert, and F. H. Joel, "Large-eddy simulations of a round jet in crossflow," J. Fluid Mech. **379**, 71–104 (1999).

[17] A. Basu and N. Mansour, "Large eddy simulation of a forced round turbulent buoyant plume in neutral surroundings," in Center for Turbulence Research Annual Research Briefs (1999).

[18] X. Zhou, K. H. Luo, and J. J. Williams, "Large-eddy simulation of a turbulent forced plume," Eur. J. Mech. B **20**, 233–254 (2001).

[19] B. Devenish, G. Rooney, and D. Thomson, "Large-eddy simulation of a buoyant plume in uniform and stably stratified environments," J. Fluid Mech. **652**, 75–103 (2010).

[20] N. Kumar, P. Mukherjee, V. K. Chalamalla, A. Dewan, and S. Balasubramanian, "Assessment of RANS-based turbulence model for forced plume dynamics in a linearly stratified environment," Comput. Fluids **235**, 105281 (2022).

[21] D. R. Mehta and B. Peter, "Design rules for small low-speed wind tunnels," Aeronaut. J. **83**(827), 443–449 (1979).

[22] K. M. Talluru, S. Armfield, N. Williamson, M. P. Kirkpatrick, and L. Milton-McGurk, "Turbulence structure of neutral and negatively buoyant jets," J. Fluid Mech. **909**, A14 (2021).

[23] G. Oster and M. Yamamoto, "Density gradient techniques," Chem. Rev. **63**, 257–268 (1963).

[24] G. Daviero, P. Roberts, and K. Maile, "Refractive index matching in large-scale stratified experiments," Exp. Fluids **31**, 119–126 (2001).

[25] A. B. McCleney, "Turbulence statistics of a buoyant jet in a stratified environment," Ph.D. thesis (The George Washington University, 2016).

[26] P. Kundu, I. Cohen, and D. Dowling, *Fluid Mechanics* (Academic Press, 2015).

[27] D. Xu and J. Chen, "Experimental study of stratified jet by simultaneous measurements of velocity and density fields," Exp. Fluids **53**, 145–162 (2012).

[28] P. Odier, J. Chen, and R. E. Ecke, "Entrainment and mixing in a laboratory model of oceanic overflow," J. Fluid Mech. **746**, 498–535 (2014).

[29] P. Doron, L. Bertuccioli, J. Katz, and T. Osborn, "Turbulence characteristics and dissipation estimates in the coastal ocean bottom boundary layer from PIV data," J. Phys. Oceanogr. **31**, 2108–2134 (2001).